Performance Assessment and Interpretation of Random Forests by Three-dimensional Visualizations

Ronny Hänsch and Olaf Hellwich
Computer Vision and Remote Sensing, Technische Universität Berlin, Marchstr.23, MAR6-5, 10587 Berlin, Germany

Keywords: Random Forest, Randomized trees, Binary decision trees, Visualization.

Abstract: Ensemble learning techniques and in particular Random Forests have been one of the most successful machine learning approaches of the last decade. Despite their success, there exist barely suitable visualizations of Random Forests, which allow a fast and accurate understanding of how well they perform a certain task and what leads to this performance. This paper proposes an exemplar-driven visualization illustrating the most important key concepts of a Random Forest classifier, namely strength and correlation of the individual trees as well as strength of the whole forest. A visual inspection of the results enables not only an easy performance evaluation but also provides further insights why this performance was achieved and how parameters of the underlying Random Forest should be changed in order to further improve the performance. Although the paper focuses on Random Forests for classification tasks, the developed framework is by no means limited to that and can be easily applied to other tree-based ensemble learning methods.

1 INTRODUCTION

Over the last years Ensemble Learning (EL) techniques gained more and more importance. Instead of trying to create a single, highly optimal learner, EL methods create many sub-optimal (base-)learners and combine their output. Depending on the type of base-learner, whether they are trained independently or not, and how their output is used to create the final system answer (e.g. by selection or fusion), the individual EL approaches have been given many names, as for example mixture of experts, consensus aggregation, bagging, boosting, arcing - to name only a few of them (see e.g. (Hänsch, 2014) for more details). The main advantages of EL techniques are: 1) Less effort has to be spent on the training of the individual learners, because they are not meant to be highly accurate; 2) Diverse base-learners with different (and potentially complementary) characteristics can be used and combined; 3) By using specific fusion techniques it is possible to find solutions that were not within the individual hypotheses space of the single base-learners.

Especially the usage of decision trees within the EL framework has shown large success. The intrinsic properties of such trees (e.g. low bias with high variance, fast induction and training, built-in feature selection, easy randomization, etc.) are in perfect accordance to the underlying principles of EL and thus naturally exploited. Consequently, many different variations have been introduced: Random Forest (Breiman, 2001), Extremely Randomized Trees (Geurts and Wehenkel, 2006), Rotation Trees (Rodriguez et al., 2006), Projection-based Random Forests (Hänsch, 2014), and many more. The work of (Breiman, 1996; Breiman, 2001) introduces Random Forests (RFs) rather as a general concept, instead of a specific algorithm. Nowadays, RFs are likely to be the most commonly used variant of combining decision trees with EL. They can be used for classification as well as regression tasks and have been applied to a vast amount of different application scenarios.

Very few effort, however, has been carried out in the direction of visualizing Random Forests. The available methods are at least partly not RF-specific and can be coarsely divided into four groups: 1) As for other machine learning methods (e.g. multi-layer perceptrons or convolutional neural networks) there are of course **abstract visualizations** of the underlying model (Figure 1(a)). However, these are rather graphical models of the general algorithmic class instead of a visualization of an individual instance of this class. 2) As for any other classification or regression technique it is possible to evaluate **result-driven visualizations** by providing a graphical interpretation of the system answer. Figure 1(b) gives an example of a classification result, that was created by a spe-

Hänsch R. and Hellwich O..
Performance Assessment and Interpretation of Random Forests by Three-dimensional Visualizations.
DOI: 10.5220/0005310901490156
In *Proceedings of the 6th International Conference on Information Visualization Theory and Applications* (IVAPP-2015), pages 149-156
ISBN: 978-989-758-088-8

cific version of an RF in (Hänsch, 2014). Since RFs are able to provide a probabilistic output (although not always used), they provide an intrinsic measure of certainty of their solution, which can be exploited in the corresponding visualization. 3) On the other hand there are **data-driven visualizations**. In (Shotton et al., 2008) RFs are used as a sophisticated clustering technique which extracts specific image features for the task of object recognition. Figure 1(c) shows to which image pattern an individual tree reacts. This visualization gives a first coarse idea about the features this method might be able to extract. Similar data-driven visualizations are available for other machine learning approaches as well, as for example for convolutional neural networks (Zeiler and Fergus, 2014). 4) The last type, **parameter-driven visualizations**, are somewhat specific to Random Forests, because they are one of the few methods that actually provide some insight how the given task is solved and do not just act as a black-box-system. The work of (Hänsch, 2014) discusses several of these properties and how they can be visualized. One example is the selection frequency of available features through the forest like it is shown in Figure 1(d) for different features (columns) per tree level (rows).

This work proposes a fifth type of visualization, which is **exemplar-driven**. It combines the visualization of the abstract model with parameter-driven visualizations and allows for deeper insights and faster understanding of the trained forest. The basic idea of the proposed method is given by the name "Random Forest" itself: If this metaphorical name suits so well as an algorithmical description, we will further extend it to a full visualization of an actual forest as it is illustrated in Figure 1(e).

2 RANDOM FORESTS

This section briefly describes the basic algorithm of Random Forests. A detailed description of RFs is beyond the scope of this work, but may be found in the literature (e.g. (Breiman, 2001)). The following discussion focuses on RFs for classification for the sake of simplicity. The method proposed here is by no means limited to that and can be applied to many other types of tree-based EL.

A Random Forest consists of many binary decision trees. These trees are inducted and trained on a training set consisting of multidimensional data points **x** and the desired system output (e.g. class label) y. The work of (Breiman, 1996) proposed that each tree has access only to a random part of the whole data set. This subset of the data enters the tree at the root node. One of the data dimensions f is randomly selected and a simple binary split is performed. An example is given by Equation 1:

$$x_f < \theta \quad (1)$$

where θ is a given threshold. All data points that fulfill this test are propagated to the left child node,

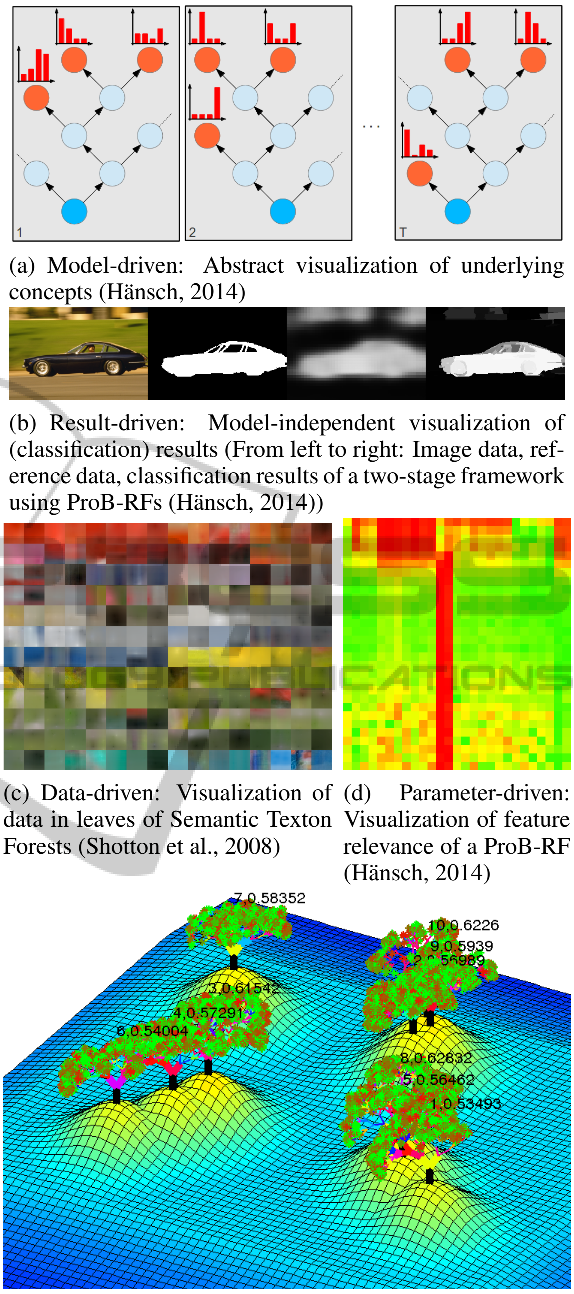

(a) Model-driven: Abstract visualization of underlying concepts (Hänsch, 2014)

(b) Result-driven: Model-independent visualization of (classification) results (From left to right: Image data, reference data, classification results of a two-stage framework using ProB-RFs (Hänsch, 2014))

(c) Data-driven: Visualization of data in leaves of Semantic Texton Forests (Shotton et al., 2008)

(d) Parameter-driven: Visualization of feature relevance of a ProB-RF (Hänsch, 2014)

(e) Exemplar-driven: Visualization of a specific RF

Figure 1: Different types of visualizing properties of a Random Forest.

all others to the right child node. The threshold θ can be defined in many ways, for example by random sampling, as median, or by criteria that optimize the purity of the child nodes with respect to the sample class distribution. This splitting is recursively performed by all nodes, but always with different data dimensions and thresholds. The recursive splitting stops if a maximal tree height is reached or too few data samples are available. In this case a terminal node (leaf) is created, which simply estimates the relative class-frequency $P_t(c|n_t)$ of the data points, that reached this leaf (node n_t of tree t).

If the class label of a query data point $\mathbf{x}$ has to be estimated, the query is propagated through all T trees of the forest beginning at the root node. Its way ends in exactly one leaf n_t in each tree t. The individual class probabilities $P_t(c|n_t)$ of those leaves are combined by a simple average (Eq. 2), which provides the final estimate of the class' a posteriori distribution.

$$P(c|\mathbf{x}) = \frac{1}{T}\sum_{t=1}^{T} P_t(c|n_t) \tag{2}$$

Unlike many other machine learning approaches, RFs not only provide measurements of the final performance (e.g. classification accuracy) but also allow insights into the actual properties of the inducted and trained trees. Some of these measurements are summarized in (Hänsch, 2014). Here, only four of the most important ones shall be mentioned, because they play a special role within the visualization process described in Section 3. The first one is the **impurity** of the nodes of each tree. Each node has access to a specific subset of the whole dataset, namely the fraction of samples that are propagated by its parent to this node. During the training process these samples provide class labels which allow the computation of a local estimate of the class distribution within this node. There are several ways to measure the impurity of a node, but the Gini impurity I as defined by Equation 3 is most commonly used.

$$I(n_t) = 1 - \sum_c P_t(c|n_t)^2 \tag{3}$$

Since the final class decision of the forest is directly based on the class estimates of the individual leaves, the impurity of the leaves is of special importance.
The work of (Breiman, 2001) argues, that for EL techniques in general and for RFs in particular, the **strength and the correlation of the individual base-learners** are two of the most important properties. Both characteristics are antagonistic to each other: On the one hand, the stronger the individual base-learners, the stronger is the whole forest. On the other hand, the higher the correlation between the base-learner, the less reasonable is it to combine several of them. There is no point in creating many trees, if they always provide the same estimate of the class label (i.e. their correlation equals one). In other words: It is important to create trees, which make as few mistakes as possible, but when they do, then it should be different mistakes. Only then the underlying principles of EL can show their full potential.

In the case of RFs, the strength of the individual trees can be nicely estimated: Since each tree is trained only on a subset of the whole dataset, the remaining Z data points can be used to estimate a so called Out-Of-Bag error, e.g. based on the 0-1-loss E_{01} as defined by Equation 4. This estimate gives a good approximation of the generalization error of the tree without the need of an additional holdout set.

$$E_{01} = \frac{1}{Z}\cdot\sum_{\mathbf{x}}(1-\delta(argmax(P_t(c|n_t)), y_{\mathbf{x}})) \tag{4}$$

The correlation $\Gamma = [\gamma_{(t_1,t_2)}] \in \mathbb{R}^{T\times T}$ of the trees is measured as their agreement during classifying the training data, i.e. $\gamma_{(t_1,t_2)}$ is the Pearson correlation coefficient of the classification results of the trees t_1 and t_2.

Last but not least, the **strength of the whole forest** is of interest. In contrast to the strength of a single tree, it should be estimated on a holdout set, since the forest as a whole has seen all samples of the training dataset. Although RFs are not prone to overfitting, the error estimate based on the training set will be biased and should not be used as an approximation of the generalization error. Instead, previously unseen samples of a test set are propagated through the forest to determine their label. A confusion matrix $\mathbf{E} \in \mathbb{R}^{C\times C}$ can be computed based on the estimated class labels as well as the labels provided by the reference data. This work uses the balanced accuracy BA defined by Equation 5 as performance measure, since it is less biased in case of imbalanced datasets.

$$BA = \frac{1}{C}\sum_{i=1}^{C}\frac{e_{cc}}{Z_c} \tag{5}$$

where C is the number of classes and Z_c the number of samples of class c and e_{cc} is the c-th entry on the main diagonal of $\mathbf{E}$.

3 VISUALIZATION

This section explains how a given RF is visualized based on its properties such as described in Section 2. The first subsection focuses on the creation of a single tree, while Subsection 3.2 describes how the whole forest is formed by multiple trees.

3.1 Tree Visualization

Each tree of an RF is a binary decision tree. There are many approaches to visualize these simple types of tree models. The method described in this paper leads to a simple three-dimensional tree-structure, that represents the underlying decision trees with respect to its topology as well as basic properties such as leaf impurity and selected features.

The root node of the tree is visualized as a vertical line (orientation angles $\alpha = 90°, \beta = 0°$). Length and direction of the two child branches L and R are based on the height h of these nodes and determined by Equations 6-7.

$$(\alpha,\beta)_{h+1}^{L/R} = (\alpha,\beta)_h \pm (30°, \kappa_1 \cdot 45°) \quad (6)$$

$$l_{h+1}^{L} = l_{h+1}^{R} = l_h \cdot f \quad (7)$$

where $f = \kappa_2 \cdot (f_{max} - f_{min}) + f_{min}$ is the shortening factor and $0 \leq \kappa_1, \kappa_2 \leq 1$ are two random numbers. The rotation of the branches allows the tree to actually grow in a three-dimensional space, while the shortening factor f leads to more natural-looking trees. The thickness of the branches is proportional to the amount of data the node contains. The color of each branch can be freely chosen to represent different properties of the corresponding node. In this paper it is the color-coded ID of the feature that was used by the tree to split the data in this node. The line of the root node is displayed in black.

The recursive growing of the tree stops as soon as a leaf node is reached. In this case an asterisk symbol is plotted, whose size and color corresponds to the amount and to the impurity of the data within this leaf, respectively (ie. red for uniform distributed class labels, green for pure nodes).

3.2 Forest Visualization

As discussed in Section 2 the classification accuracy of the whole forest as well as strength and correlation of the individual trees are the most important characteristics of an RF. Within this work all three of them are represented by the spatial layout of the forest.

The relative spatial (2D) position of two trees of the visualized forest is chosen to represent the correlation of the two corresponding trees of the RF. In order to transform the provided correlation matrix $\Gamma \in \mathbb{R}^{T \times T}$ into a set of T $2D$ positions, each tree t is assigned with a two-dimensional voting space $V_t \in \mathbb{R}^{N_x \times N_y}$, where N_x, N_y are the spatial dimensions of the visualization and T the number of trees. The proposed algorithm (summarized by Algorithm 1) selects in each iteration $i = 1, ..., T$ the strongest, not yet processed tree (i.e. with the smallest OOB-error, see Section 2). If $i = 1$, the position p_t of the first tree is initialized as the center of the spatial layout (i.e. $p_t = (N_x/2, N_y/2)$). The currently selected tree votes for possible positions of all other trees by updating the corresponding voting space using Equation 8.

Algorithm 1: Position Voting.

```
Require: Correlation matrix Γ, tree strength, forest
    strength
  for $i = 1$ to $T$ do
    Select strongest, non-processed tree $t$
    if $i == 1$ then
      $(x,y)_t = (\frac{N_x}{2}, \frac{N_x}{2})$
    else
      $(x,y)_t = \arg\max(V_t)$
    end if
    for $j = 1$ to $T$ do
      if $j \neq t$ then
        Update voting space $V_j$ (Equation 8)
      end if
    end for
  end for
```

$$\begin{aligned} V_j &= V_j + v \otimes g & (8) \\ v(x,y) &= \begin{cases} 1 & \text{, if } |r(x,y) - d(x,y)| < w \\ 0 & \text{, otherwise.} \end{cases} & (9) \\ d &= (1 - \gamma_{t,j}) \cdot r_{max} + r_{min} & (10) \\ r(x,y) &= ||(x,y) - (x,y)_t|| & (11) \end{aligned}$$

where $\otimes$ means convolution and g is a $2D$ Gaussian function. Basically, v corresponds to a ring of width w around the position of the current tree t within the voting space V_j, where the radius of the ring is inverse proportional to the correlation $\gamma_{t,j}$ between the two trees. Thus, two highly correlating trees are more likely to be close to each other within the visualization. In order to prevent a too strong spatial overlap in the case of very similar trees (e.g. $\gamma = 1$) a minimum distance r_{min} is enforced.

For all subsequent trees the position is randomly sampled from the maximal values within the corresponding voting space V_t.

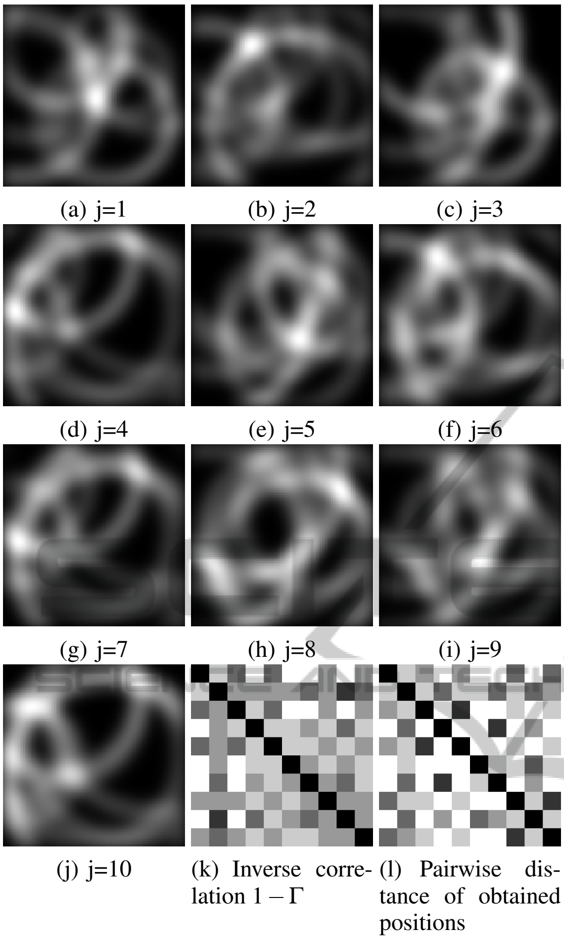

Figure 2: Voting space to sample spatial positions based on correlation.

Figures 2(a)-2(j) show an example of this voting space based on a forest of $T = 10$ trees. Figure 2(k) and Figure 2(l) show the inverse of the provided correlation matrix $1-\Gamma$ and the pairwise distance matrix $D(i, j) = ||(x, y)_i - (x, y)_j||, (i, j = 1, ..., 10)$ of the calculated positions, respectively. As can be seen both matrices are very similar with a correlation coefficient of $\rho = 0.86$ and a p-value $<< 0.001$, which shows that the proposed method of converting a given correlation matrix into a set of spatial 2D positions works sufficiently well.

The whole forest is positioned on a plateau with a height that is proportional to the balanced classification accuracy *BA* (Equation 5) of the whole forest. The borders of the plateau decrease smoothly to the zero-level for the sake of visual beauty. Furthermore, each tree of the forest stands on a local hill. The height of this hill corresponds to the individual strength of this tree as estimated based on the OOB-error (Equation 4).

4 EXAMPLES

This section shows visualizations of several, specific instances of Random Forests. The same RF-framework is used, however, the forests were generated with different parameter settings. All RFs of this section are trained for land cover classification from Polarimetric Synthetic Aperture Radar (PolSAR) images. The reference data contains five different classes, namely Forest, Shrubland, Field, Roads, and Urban area. The exact details of this classification task are of no particular interest for the discussion of this paper, but can be found in (Hänsch, 2014). Instead, this section focuses on the possible insights into problems and solutions as they are provided by the proposed visualization method. While Subsection 4.1 starts with a discussion on single trees, Subsection 4.2 shows additional visual information based on the whole forest.

4.1 Single Trees

Figure 3 shows four different examples of a Random Forest, where the maximal tree height was set to five, only one test per node is created, and the split point (i.e. θ in Equation 1) is sampled uniformly from the interval defined by the minimal and maximal values of the randomly selected data dimension. The trees show extremely weak performance with an average 0-1-loss of 57%. Figure 3 gives a visual explanation for one of the major reasons for this low accuracy: The approach of creating only one test and to uniformly sample the split point does not perform any task-specific optimization. Consequently, there is a

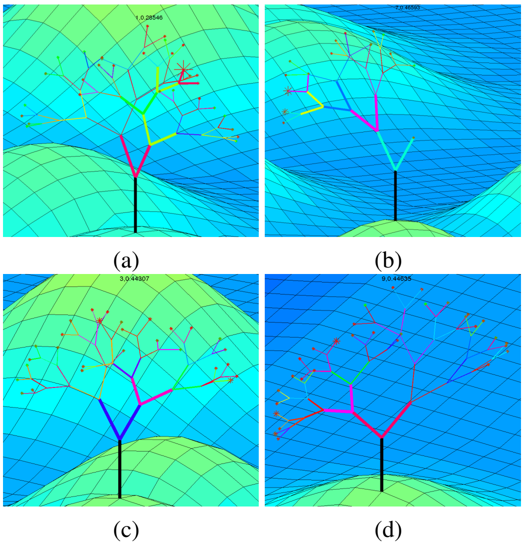

Figure 3: Extremely weak trees (Maximal height: 5; Uniform sampled split point; One test per node).

very high risk of creating a weak split, i.e. a split which propagated only a small fraction of the data to one of the child nodes. Since the maximal tree height is set to five, only a few splits are possible. If most of them are unbalanced, very large and impure leaves are created which contain the major part of the data. Figure 3(a)-3(b) show examples of this problem. Even if the created splits are more or less balanced, there are too few of them (due to the small maximal tree height) and they are too less optimized (due to uniform sampled split points). Figure 3(c)-3(d) show examples of such trees, where the leaves are of similar size but with high impurity.

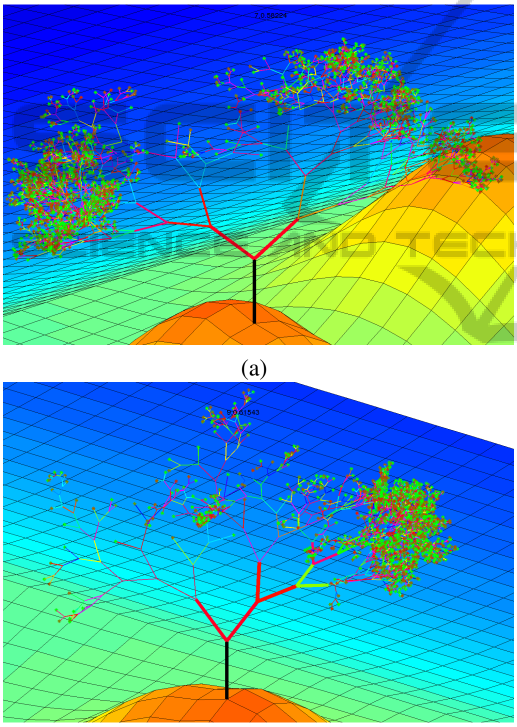
(a)

(b)

Figure 4: Strong trees (Maximal height: 45; Uniform sampled split point; One test per node).

One possible solution for this problem is to simply increase the maximal tree height. Figure 4 shows two exemplary trees of a Random Forest, where the maximal tree height was increased to 45, while the remaining parameters stayed unchanged. There are still imbalanced splits as for example the split of the root node in Figure 4(b). However, due to the considerably higher maximal height, there are enough possibilities to create well-balanced splits. The number of impure leaves does consequently decrease dramatically, while the strength increases (the 0-1-loss falls from 57% to 39%). Nevertheless, there are still a considerable amount of unbalanced splits (see e.g. first branches of tree in Figure 4(b)) as well as weakly optimized leaves (many small, red leaves in Figure 4(a)).

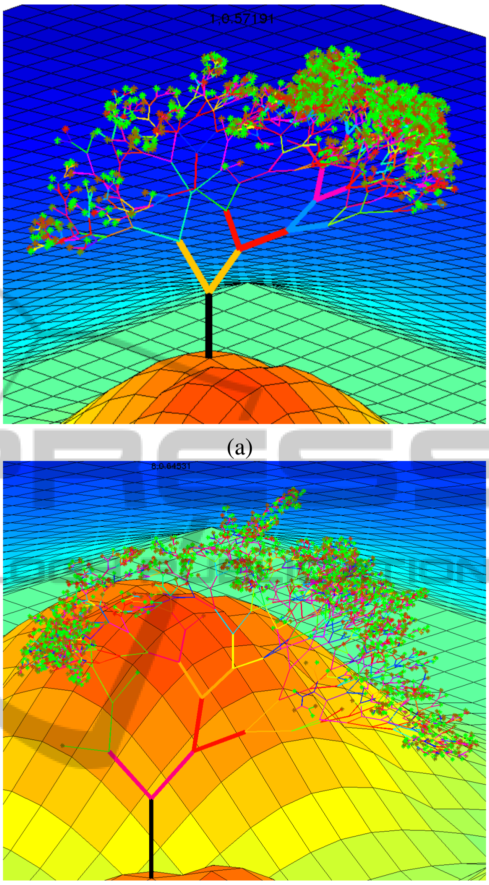

(a)

(b)

Figure 5: Strong trees (Maximal height: 45; Gini-optimized split point; One test per node)

The small size of the leaves of the trees depicted in Figure 4 indicate, that the performance of the RF cannot be further increased by increasing the maximal height of its trees. Instead, a larger amount of optimization has to be introduced during tree induction. One way to achieve that is to optimize the split point with respect to the impurity of the resulting child nodes instead of selecting it randomly. The Gini-impurity (Equation 3) is commonly used for this purpose. This decreases the risk of selecting weak split points and can lead to an increase of performance. The trees in Figure 5 have been created with the Gini-optimized split point selection and a maximal tree height of 45. They show considerably less red leaves than the trees in Figure 4. However, it does not change the risk of selecting a bad splitting dimension as is illustrated in Figure 5(b) (first splits after root node).

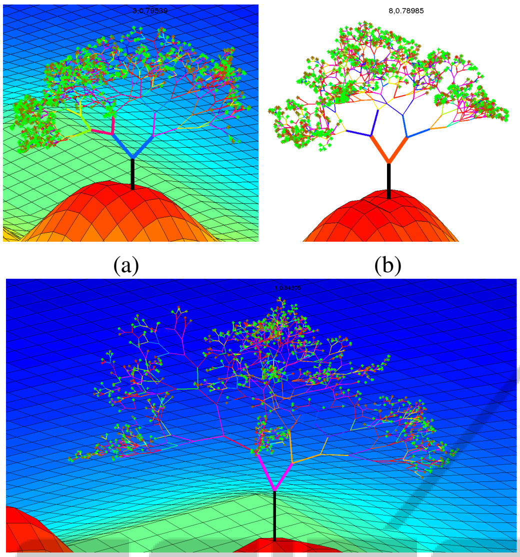
(a) (b)

(c)

Figure 6: Very strong trees (Maximal height: 45; Median-based split point; Ten tests per node).

Figure 6 shows three examples with the highest degree of optimization used in this section. The split point is defined as the median of the data in each node, which leads to very balanced splits. The maximal tree height was set to 45 allowing for as many (balanced) splits as possible for the used dataset and a maximal information extraction. Furthermore, each node created ten different tests (i.e. selected ten different splitting dimensions) and selected the best split (based on the Gini-impurity of the child nodes). Consequently, the individual nodes as well as the whole tree is relatively balanced, as can be seen in Figure 6. The individual strength (measured as $1 - E_{01}$) of these trees is with 0.8 the highest of all tree examples of this section, which is illustrated by the high hills on which the trees are located.

4.2 Forest

While the previous section discussed properties of individual trees, the current section brings these trees into the context of the whole forest. Each tree is already given with its $3D$ layout, which is controlled by the recursive splitting process during tree induction (shape/color of the tree), the impurity of the leaf nodes after tree training (color/size of leaves), as well as the strength of the tree measured as out-of-bag 0-1-loss during tree evaluation (height of the local hill of the tree). The two properties that remain to be visualized are the strength of the whole forest as well as the correlation between the individual trees.

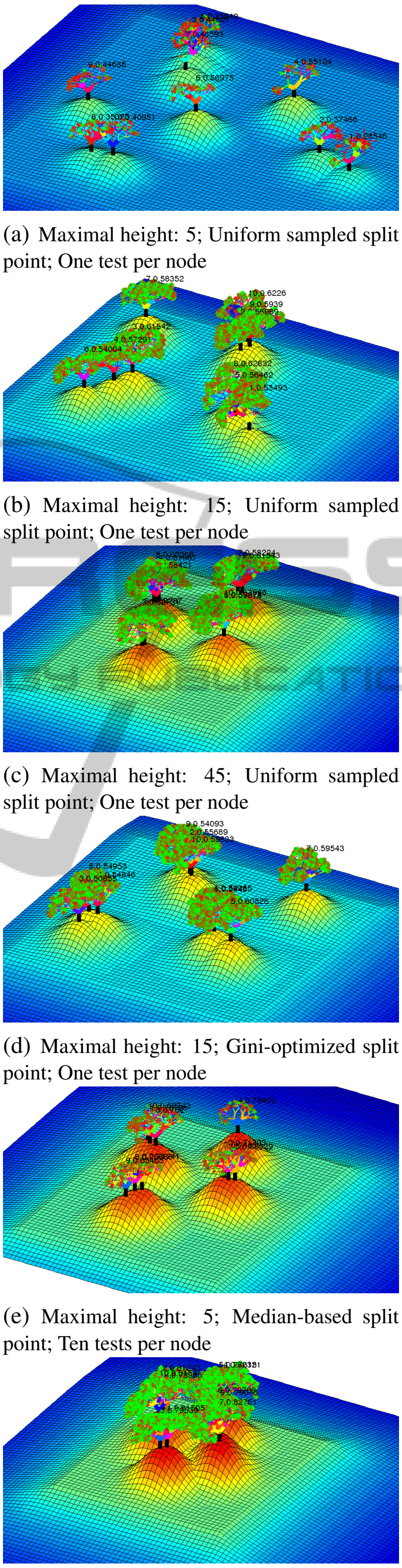
(a) Maximal height: 5; Uniform sampled split point; One test per node

(b) Maximal height: 15; Uniform sampled split point; One test per node

(c) Maximal height: 45; Uniform sampled split point; One test per node

(d) Maximal height: 15; Gini-optimized split point; One test per node

(e) Maximal height: 5; Median-based split point; Ten tests per node

(f) Maximal height: 45; Median-based split point; Ten tests per node

Figure 7: Forest examples.

Figure 7(a)-7(c) show RFs with uniform sampled split points, one test per node, and a maximal tree height of 5, 15, and 45, respectively. Four key characteristics of the increase of the maximal tree height are immediately evident: 1) The decision trees become larger and more complex as visualized by height and shape of the displayed trees. 2) The trees become stronger as visualized by the height of the local hill (0-1-loss decreases from 54% to 39%). 3) The performance of the whole RF increases as well (BA increases from 54% to 93%), which is visualized by the height of the global plateau. 4) The trees correlate more and more with each other (average correlation increases from 0.4 to 0.84) and are consequently located closer to each other.

Figure 7(d) shows an RF with Gini-optimized split point selection and a maximal tree height of 15. Compared to an RF with similar parameter setting but uniform sampled split points, the performance increased from 66% to 71%, which is visualized by a slightly higher plateau. Figure 7(e)-7(f) show an RF with median-based split point definition, best-of-ten test selection, as well as a maximal tree height of 5 and 45, respectively. The advantage of this tree induction scheme is immediately evident if the visualization in Figure 7(e) is compared to the visualizations of the other RFs of this section. Already at this shallow maximal tree height, it outperforms other RFs as can be clearly seen by the height of the global plateau and local hills. Both, individual as well as global performance, increase with higher trees: The BA increases from 90% to 95% (leading to a slightly higher plateau in Figure 7(f) than in Figure 7(e)). The average strength of the trees increases, i.e. the tree error decreases from 0.28 to 0.20 (resulting in higher local hills). Also the correlation increases from 0.79 to 0.92 on average, which leads to a very dense forest in Figure 7(f). Figure 8(a)-8(b) visualize the same RF as in Figure 7(f) from different viewing directions.

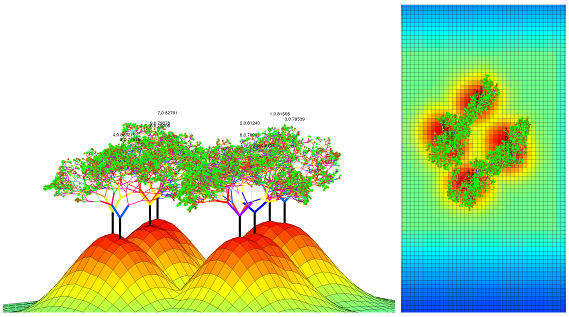

(a) (b)

Figure 8: Different views of one forest (Maximal height: 45; Median-based split point; Ten tests per node).

5 CONCLUSIONS

This work introduced a novel technique to visualize one of the most successful machine learning approaches. Unlike other methods to visualize certain properties of Random Forests, the current work is neither completely abstract, nor completely data-driven, but instead combines both categories to a exemplar-driven visualization. Besides only illustrating the underlying principle of decision trees, it visualizes a specific, given Random Forest. Many of the main properties of a Random Forest including individual tree strength and correlation as well as the strength of the whole forest are dominant visual characteristics and allow a fast and accurate judgement of the general performance of the underlying RF classifier. An analysis of shape and color of the individual trees allows to infer knowledge about unfavorable parameter settings and provide cues for adjustments in order to increase performance.

Future work will mainly focus on a higher advanced graphical user interface, which allows to blend in more information about the Random Forest at hand and to switch easily between different modes of visualization (e.g. single tree, 1*D* sorted trees, spatially arranged trees, etc.). Furthermore, an online visualization which visualizes the RF during tree induction and training can be beneficial to gain an even deeper understanding of the learning part which eventually might lead to new theoretical insights about RFs in particular and EL in general.

REFERENCES

Breiman, L. (1996). Bagging predictors. In *Machine Learning*, pages 123–140.

Breiman, L. (2001). Random forests. *Machine Learning*, 45(1):5–32.

Geurts, P. and Wehenkel, D. E. L. (2006). Extremely randomized trees. *Machine Learning*, 63(1):3–42.

Hänsch, R. (2014). *Generic object categorization in PolSAR images - and beyond*. PhD thesis.

Rodriguez, J. J., Kuncheva, L. I., and Alonso, C. J. (2006). Rotation forest: A new classifier ensemble method. *IEEE Transactions on Pattern Analysis and Machine Intelligence*, 28(10):1619–1630.

Shotton, J., Johnson, M., and Cipolla, R. (2008). Semantic texton forests for image categorization and segmentation. In *IEEE Conference on Computer Vision and Pattern Recognition*, pages 1–8.

Zeiler, M. D. and Fergus, R. (2014). Visualizing and understanding convolutional networks. In *Computer Vision ECCV 2014*, volume 8689 of *Lecture Notes in Computer Science*, pages 818–833.